

# Simulated Optimisation of a 10 mJ Class, mid-IR Driven Laser Wakefield Accelerator Demonstrating a High Charge, MeV Electron Source Created via Extreme Laser Redshifting

Contact: [jonathan.wood08@imperial.ac.uk](mailto:jonathan.wood08@imperial.ac.uk)

J. C. Wood, S. P. D. Mangles and Z. Najmudin

The John Adams Institute for Accelerator Science, Imperial College London, London, SW7 2AZ, United Kingdom

## Abstract

The development of high power, few-cycle pulses of mid-infrared laser light presents new opportunities for Laser Wakefield Accelerators, which are discussed from first principles. Principally, the accelerating structure is much larger than what can be driven using comparable 0.8 μm systems, presenting improved opportunities for probing with light or particle beams. This may also lead to the acceleration of higher charge beams. It is shown via particle-in-cell simulations that a 25 mJ, 30 fs pulse of 4 μm light can accelerate self-injected electrons to 20 – 40 MeV in a millimetre scale target. This highlights an additional advantage of long wavelength drivers: they do not need the small, precision engineered targets associated with short wavelength systems. For ratios of plasma density to critical density  $n_e/n_c \gtrsim 0.05$ , 2D and 3D simulations show the formation of a post-soliton after the initial electron acceleration due to pulse depletion and redshifting. As the post-soliton forms, a large amount of charge is injected into it and accelerated to multi-MeV levels.

## 1 Introduction

Laser Wakefield Acceleration (LWFA) is an electron acceleration technique where electrons gain energy from the large electric fields present in a nonlinear plasma wave [1, 2]. An intense, ultrashort laser pulse can drive a plasma wave in its wake via the ponderomotive force  $F_p \propto -\nabla a^2$ , where the normalised vector potential  $a = eA/m_ec$ . As the laser pulse propagates through an underdense plasma it pushes electrons away from regions of high intensity, setting up a charge oscillation which travels behind the laser pulse at close to the speed of light  $c$ . For  $a_0 \gtrsim 2$  all electrons can be blown out from the first wakefield period [3, 4], or ‘bubble’, resulting in fields of order 100 GV m<sup>-1</sup>. This is greater than 1000 times the breakdown limit of conventional particle accelerators, meaning LWFA is attractive as a compact source of high energy electrons. It has been shown that LWFAs can accelerate electrons to GeV energies in centimetre scale plasmas [5–8]. The maximum energy gain is limited by dephasing, where the electrons travelling very close to  $c$  outrun the accelerating fields of the wakefield which move at approximately the plasma group velocity  $v_g < c$ , or by the depletion of the laser energy.

At the energy frontier of LWFA, lasers with powers of order 100 TW to 1 PW are required. At the other end of the energy scale, MeV scale LWFAs can be driven by laser pulses containing only a few millijoules of energy [9–12]. Additionally, these low energy ultrafast lasers can run at kilohertz repetition rates, comparing favourably to current high power systems that run at 0.1–1 Hz. In this Report we present results of LWFA simulations utilising a 25 mJ, 30 fs, 4 μm central wavelength laser pulse, based on the specifications of the 10 Hz Chimera laser system being built at Imperial College London. A simulation campaign based on two dimensional particle-in-cell (PIC) codes revealed the optimal plasma parameters for driving a self-injecting LWFA, suggesting that this could be a tabletop source of 20–40 MeV electron beams. In addition, we find that for sufficiently high plasma densities there is an extreme red-shift of the photons driving the wakefield, such that there is a significant electric field and  $a_0$  associated with this light. Some of the light becomes so redshifted that the plasma becomes opaque to it and it becomes trapped in an approximately stationary bubble. A large population of electrons is injected into this bubble and is accelerated up to 5 MeV, suggesting that this could be a bright source of few MeV electrons.

## 2 Physics Considerations for a LWFA with a Mid-Infrared Laser

Long wavelength laser drivers may be attractive for several applications because of the favourable scaling of  $a_0$  with wavelength  $\lambda$ ,  $a_0 \propto \sqrt{I\lambda^2}$ , where  $I$  is the laser intensity. The energy  $\mathcal{E}$  of a laser pulse with area  $\pi w_0^2$  and duration  $\tau$  is given by  $\mathcal{E} \approx I\pi w_0^2 \tau \propto (a_0^2/\lambda^2)w_0^2\tau$ . In a LWFA the pulse length should be matched to the plasma wavelength  $\lambda_p$  in all 3 dimensions to drive a strong wakefield. Therefore,

$$\mathcal{E} \propto a_0^2 \lambda_p^3 / \lambda^2 = a_0^2 (n_c/n_e) n_e^{-1/2}, \quad (1)$$

where  $n_e$  is the plasma number density and  $n_c = \epsilon_0 m_e \omega^2 / e^2$  is the critical density for light of frequency  $\omega$ .

The maximum electron energy gain in a nonlinear LWFA is given by

$$\Delta W = \frac{2}{3} a_0 \frac{n_c}{n_e} m_e c^2 = \frac{2}{3} a_0 \gamma_{ph}^2 m_e c^2, \quad (2)$$

where  $\gamma_{ph}$  is the Lorentz factor associated with the wakefield phase velocity, or in a linear LWFA by  $\Delta W \simeq a_0^2(n_c/n_e)m_ec^2$  [13]. Enforcing a constant  $\Delta W$  via keeping  $a_0$  and  $n_c/n_e$  the same implies  $n_e \propto 1/\lambda^2$ , and reduces the laser energy scaling in eq. 1 to  $\mathcal{E} \propto \lambda$ , which appears prohibitive for long wavelength systems. There are, however, multiple advantages to using long wavelength drivers. Having  $n_e \propto 1/\lambda^2$  implies that the plasma wavelength  $\lambda_p \propto \lambda$ , meaning that a large wake-field bubble can be driven, which would be beneficial for optical or particle beam probing. Ultrafast optical probing has been shown to reveal the injection dynamics of a LWFA [14, 15], although only at relatively low resolution so far. Meanwhile, particle beam probes can be used to map the electromagnetic fields of a wakefield [16], which would be significantly easier to achieve for large bubbles.

We also note that the dephasing length  $L_d = (4/3)(n_c/n_e)a_0/k_p$  [13], where  $k_p$  is the plasma wavenumber, has a  $L_d \propto \lambda$  scaling for constant  $a_0$  and  $n_c/n_e$ . The comparatively long dephasing lengths with longer  $\lambda$  is an additional advantage of long wavelength LWFA drivers because targets can be produced without the need for microscale manufacturing. This is particularly important when using lower energy, tabletop laser systems.

Finally, the large bubble driven by longer  $\lambda$  systems has been shown via simulations to be beneficial for trapping more charge [17]. From Lu et al., [13], the number of accelerated electrons  $N_e \propto \lambda\sqrt{P}$ , where  $P$  is the laser power. So while a higher energy laser pulse is required to obtain the same electron energy, this is compensated for by the higher injected charge, and the efficiency of the accelerator is not compromised. Indeed, this could be a route to producing the higher charge, low energy spread beams required for proposed applications of LWFAs such as drivers of compact free-electron lasers.

### 3 Simulations of the Performance of the 4 μm Chimera System as a LWFA Driver

In the simplest experimental regime, a laser pulse can be self-guided over many Rayleigh lengths within the plasma due to the relativistically nonlinear refractive index of the plasma. This occurs for powers greater than the critical power  $P > P_c \approx 17(n_e/n_e)$  GW [18]. For the Chimera laser pulse this sets a minimum plasma density  $n_{e,min} = 1.4 \times 10^{18} \text{ cm}^{-3}$ , corresponding to a reasonably high  $n_e/n_c = 0.02$ . To ensure that we simulate a blowout regime LWFA we impose  $a_0 = 2$ , corresponding to a peak intensity  $I_0 = 3.4 \times 10^{17} \text{ W cm}^{-2}$ . This can be achieved by focussing the pulse to a FWHM spot size of 14.2 μm. Noting that the pulse length  $c\tau_{FWHM} = 9.0 \mu\text{m}$ , we see that we have an ideal pulse for accessing the blown out LWFA regime, as the bubble size can be closely matched to the

laser size in all three dimensions. Using an optimum  $n_e = 1.6 \times 10^{18} \text{ cm}^{-3}$  estimated from the matched spot size condition  $k_p w_0 = 2\sqrt{a_0}$  [13], we estimate  $\Delta W = 31 \text{ MeV}$  and  $L_d = 360 \mu\text{m}$ . An 800 nm driver of an equivalent system would have  $L_d = 72 \mu\text{m}$ , which highlights the benefits of mid-infrared laser drivers with regards to target requirements.

To study the potential of Chimera as LWFA driver more thoroughly, 2D PIC simulations were performed in the EPOCH code [19], using a 25 mJ, 30 fs FWHM duration, 4 μm wavelength laser focussed to a spot size to ensure either  $a_0 = 2.0$  or  $a_0 = 1.5$  in vacuum, depending on the run.  $n_e$  was varied in the range  $1.5 - 10 \times 10^{18} \text{ cm}^{-3}$ . The plasma profile had a 100 μm linear ramp at the start and end. Lower density simulations had 2 mm plasma lengths, higher density simulations had 1 mm plasma lengths, although generally the plasma length was set to be significantly longer than  $L_d$  so that a plasma length scan could be carried out in a single simulation. The laser was focussed at the top of the density up-ramp. The simulations used a box size of 200 μm longitudinally and 120 μm transversely with 60 and 20 cells per laser wavelength respectively, with 4 particles per cell.

Figure 1 shows the maximum electron longitudinal momentum  $p_x$ , injected charge and the optimal accelerator length as a function of  $n_e$ . These simulations were performed in a self-guided, self-injecting regime. No self-injection was observed below  $n_e = 2 \times 10^{18} \text{ cm}^{-3}$  for  $a_0 = 2$ , or for  $n_e < 3 \times 10^{18} \text{ cm}^{-3}$  for  $a_0 = 1.5$ . The peak electron momentum approximately follows the expected  $\Delta W \propto 1/n_e$  trend with  $a_0 = 4$ , suggesting that significant pulse evolution via self-focussing and self-compression was required to inject charge. While acceleration above 40 MeV was observed, only a very low charge was trapped in the wakefield in this case. Therefore the best operating parameters for  $a_0 = 2$  was in the density range  $3 - 4 \times 10^{18} \text{ cm}^{-3}$ , where we saw acceleration to  $p_x = 20 - 30 \text{ MeV/c}$  from  $0.6 - 0.7 \text{ mm}$  length targets. At an optimal  $n_e = 2.8 \times 10^{18} \text{ cm}^{-3}$  a low momentum spread bunch was observed, with a full width in  $p_x$  of 4 MeV/c centered on 18 MeV/c.

### 4 Simulations Showing Extreme Red-shifting

As the laser pulse drives a wakefield it creates a positive density gradient at the front of the pulse, which corresponds to a negative refractive index gradient. Via the process of photon acceleration [20, 21], this causes a redshift of the photons at the front of the pulse. Higher  $n_e/n_c$  plasmas result in higher refractive index gradients and thus a greater redshifting of the drive laser. Due to the low laser power we are considering, we find ourselves driving wakefields in a relatively high density regime. First we consider a 2D simulation of a fully ionised plasma, with no dopant, of density  $n_e =$

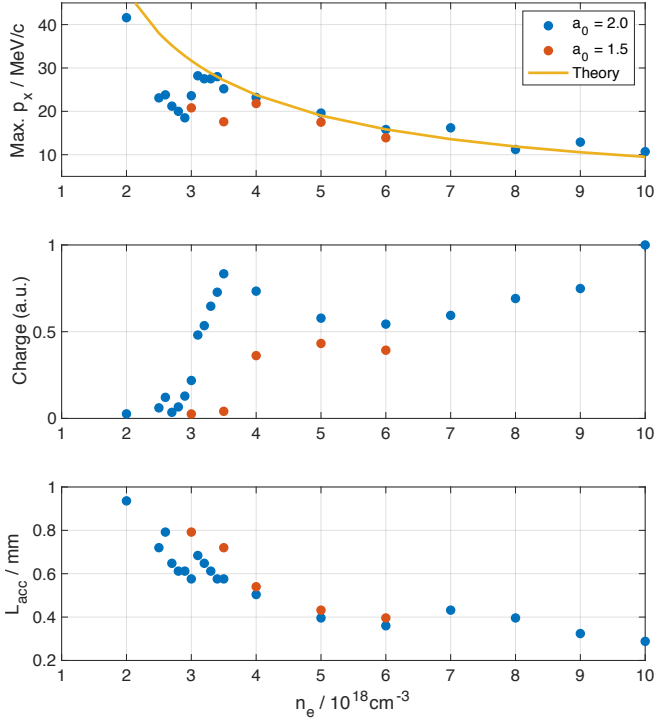


Figure 1: Results of the optimisation scan as a function of  $n_e$ , for vacuum  $a_0$  values of 1.5 and 2.0. (a) Maximum  $p_x$  found at any point in the simulation, and estimated from eq. 2 with  $a_0 = 4$ . (b) Maximum charge accelerated beyond  $p_x = 5.0 \text{ MeV}/c$ . (c) Plasma length at which the electron  $p_x$  was maximal.

$2.8 \times 10^{18} \text{ cm}^{-3}$ . The plasma was  $800 \mu\text{m}$  long with  $100 \mu\text{m}$  linear density ramps at the start and end. The laser was polarised out of the simulation plane (i.e. in the  $z$  direction). We use a  $4 \mu\text{m}$ ,  $a_0 = 2$  laser driver as described previously, although the physics demonstrated in the following does not depend on  $\lambda$ , and only on  $n_e/n_c$  and  $a_0$ .  $n_e$  and the electric field in the  $z$  direction,  $E_z$ , are plotted at a range of times in Figure 2. In the initial part of the simulation the laser drives a blown out wakefield, and a small amount of charge is injected into the second wakefield bucket, evidenced by the  $t = 1.32 \text{ ps}$  data. As it drives the wakefield the laser begins to redshift, and the long wavelength light falls backwards in the frame comoving with the initial pulse at the linear group velocity. As evidenced by the  $t = 1.92 \text{ ps}$  data, the redshifted light has a large electric field amplitude, and this acts to elongate the back of the bubble. By  $t = 2.16 \text{ ps}$  the short wavelength light has significantly depleted in energy and drives only a low amplitude wakefield, while the high field long wavelength light starts to drive a blown out wakefield which rapidly falls backwards in the moving window. Lowering the wakefield velocity makes it easier to trap charge [22], and an injection of electrons is witnessed by  $t = 2.46 \text{ ps}$ . Very severe redshifting is also seen at this time, where the longest

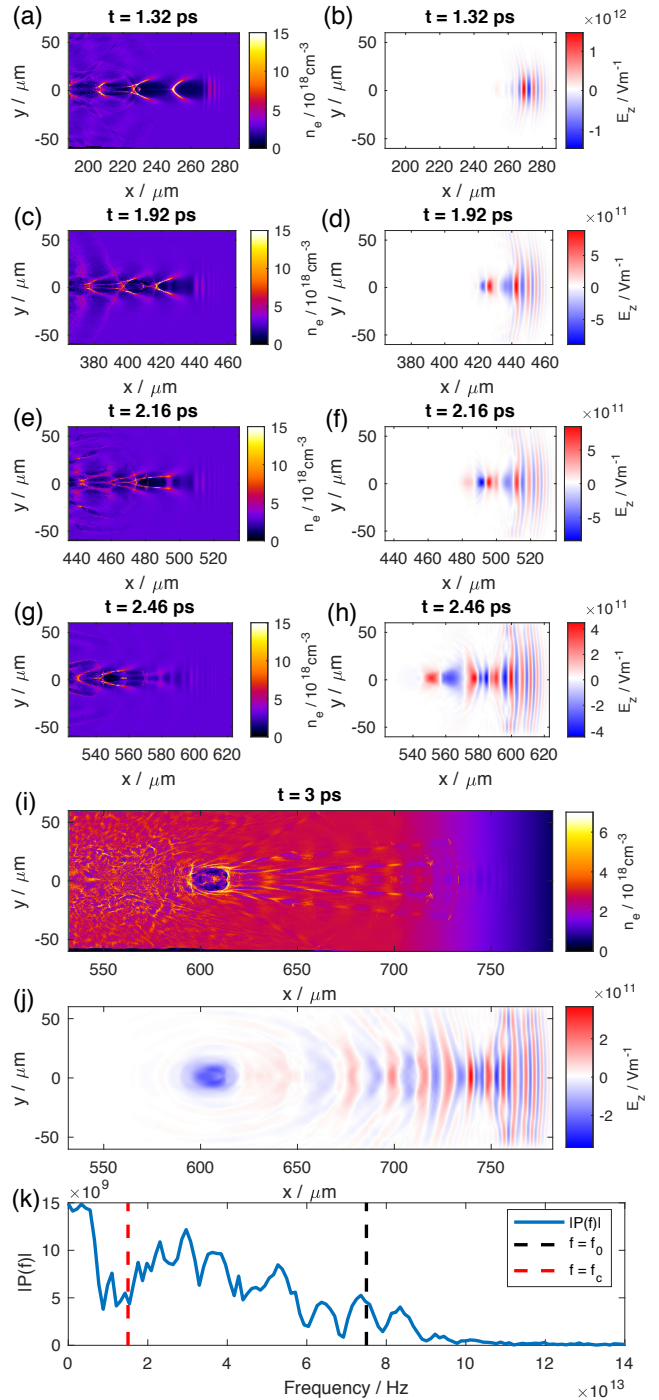


Figure 2: 2D simulation results demonstrating extreme redshifting of the drive pulse in a LWFA, resulting in postsoliton formation and the injection of charge.  $n_e$  is plotted in (a), (c), (e), (g) and (i), and  $E_z$  is plotted in (b), (d), (f), (h) and (j), at simulation times of  $1.32 \text{ ps}$ ,  $1.92 \text{ ps}$ ,  $2.16 \text{ ps}$ ,  $2.46 \text{ ps}$  and  $3.00 \text{ ps}$ . (k) plots the spectrum of  $E_z$  at  $t = 3.00 \text{ ps}$ , where the black line shows the original central frequency  $f_0$  and the red line shows the critical frequency  $f_c$ .

wavelength is approaching  $10\text{ }\mu\text{m}$ . The strong redshifting continues, and by  $t = 3.0\text{ ps}$  some light has a wavelength long enough that it finds itself surrounded by critical density plasma and its group velocity becomes zero, as evidenced by the spectral plot in Fig. 2 (k). This triggers a large injection of charge. Since  $\gamma_{ph} = 1$ , we expect modest energy gains of only a few MeV from equation 2. Figure 3 plots the electron momentum spectrum and accelerated charge for a range of simulation times. It dis-

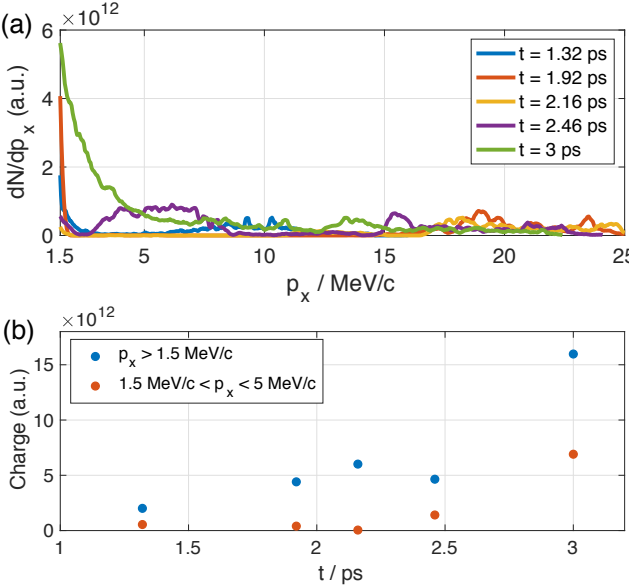


Figure 3: Electron momentum spectra, (a), and total accelerated charge, (b), for all electrons with  $p_x > 1.5\text{ MeV}/c$  and in the range  $1.5\text{ MeV}/c < p_x < 5.0\text{ MeV}/c$ , at a selection of simulation times.

plays prominent injection events due to large redshifting at  $t = 2.46\text{ ps}$  and as the bubble ‘stops’ at  $t = 3.0\text{ ps}$ . Integration of the spectra to determine the total injected charge with  $p_x > 1.5\text{ MeV}$  reveals that the total charge increases by a factor of 3 when the bubble stops, as shown in Fig. 3 (b), making this a high flux source of few MeV electrons. The low momentum cut-off was chosen to exclude the electrons that make up the plasma wave.

This effect was not observed for  $n_e/n_c \lesssim 0.04$ , but was observed in multiple simulations up to at least  $n_e/n_c = 0.14$ . The long wavelength pulse was trapped in a region evacuated of plasma electrons, creating a feature that persisted for at least  $0.9\text{ ps}$ , although electrons were only injected during its formation. It also did not occur when the laser pulse was polarised in the plane of the simulation.

These features are similar to previous reports of postsoliton formation, e.g. [23, 24], where redshifted light becomes trapped in the plasma and expels electrons from a  $c/\omega_p$  sized region. Not present in the simulations here are the ion effects. When these are included, postsolitons

expand slowly over time due to the Coulomb repulsion of the ions. Additionally the static electric field accelerates fast ions within the postsoliton structure [23].

Since this effect occurs in 2D simulations where the laser is polarised out of plane, and not at all when it is polarised in plane, a more complicated behaviour must occur in 3D. 3D simulations were performed in EPOCH with 30 cells per laser wavelength in the longitudinal direction and 6 cells per laser wavelength in both transverse dimensions, using 2 particles per cell. The laser was polarised along the  $z$  axis, and had the same characteristics as in the 2D simulations. At  $n_e = 2.8 \times 10^{18}\text{ cm}^{-3}$  and at late times, the redshifted light causes the bubble to elongate significantly, and it maintained a larger transverse extent in the  $x - y$  plane than in the  $x - z$  plane, as expected from the 2D results and as seen in [24]. However the wakefield velocity did not reduce to near zero, nor was any charge injected, possibly because the long wavelength light was not guided over a long distance.

The simulation was re-run with a higher density of  $n_e = 4.0 \times 10^{18}\text{ cm}^{-3}$ . An electron beam was quickly self-injected in to the blown out wakefield and accelerated with a broad bandwidth up to a peak  $p_x = 30\text{ MeV}/c$  after a plasma length of  $250\text{ }\mu\text{m}$ . Red-shifted light with a significant amplitude was apparent after  $300\text{ }\mu\text{m}$  of laser propagation in the simulation. Figure 4 plots the number density, laser electric field, the  $x - p_x$  phase space of the electrons and the electron momentum spectrum 1.6 ps in to the simulation. It is clear from Fig. 4 (a)-(c) that the  $4\text{ }\mu\text{m}$  light has depleted greatly in intensity and no longer drives a high amplitude wakefield. It is now the intense red-shifted light that drives the wakefield, which is significantly extended in the longitudinal direction, indicating that the phase velocity of the back of the bubble is reducing. As expected from the 2D simulation results this is associated with an injection and acceleration of a significant number of electrons to a few MeV. This is evidenced in the  $x - p_x$  phase space around  $x = 400\text{ }\mu\text{m}$ . The electron momentum spectrum in Fig. 4 (e) confirms a high charge of electrons with longitudinal momenta up to  $5\text{ MeV}/c$ . The population of few MeV electrons behind the initially injected, high energy bunch persists for  $100\text{ }\mu\text{m}$  of propagation in the plasma, indicating that these electrons could be extracted from the wakefield accelerator for applications, provided that the length of the accelerator is well controlled.

The multiple bubble structure following the first wakefield bubble in Fig. 5 (b) is qualitatively similar to previous experimental images of postsoliton formation [24]. These density structures, which present as partially cavitated bubbles, were observed in the simulation to maintain an approximately constant position in the lab frame with time. They persist for a large fraction of a picosecond at least, and the partial cavitation suggests a large amplitude trapped electric field from the red-shifted laser light. In summary, the 3D simulation demonstrates that via extreme red-shifting of the drive laser light that post-

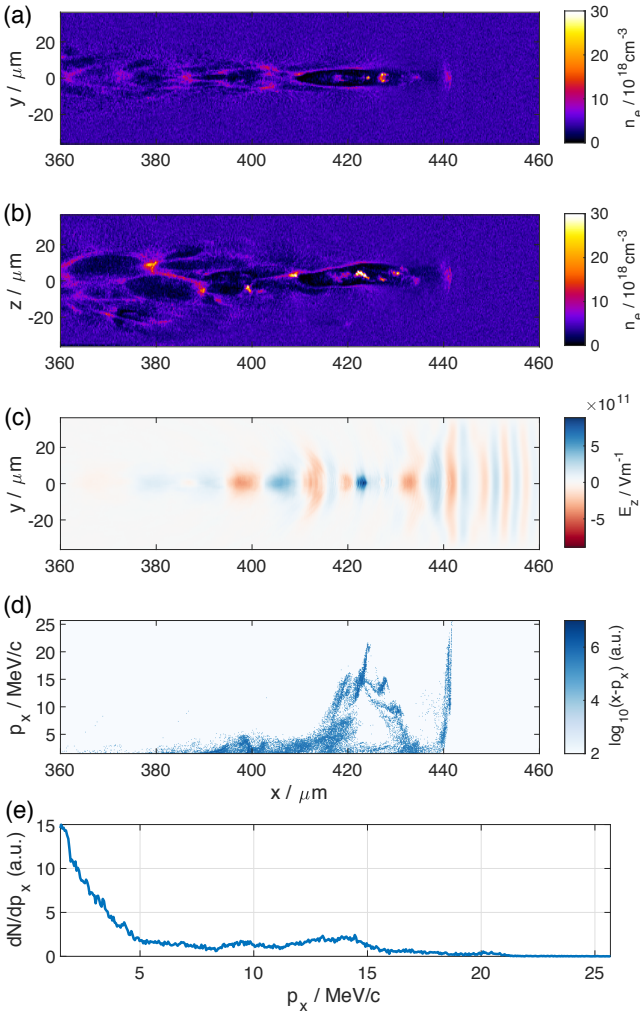


Figure 4: Results of a 3D simulation at 1.6 ps into the interaction of a Chimera laser pulse with a plasma density of  $4 \times 10^{18} \text{ cm}^{-3}$ . (a) and (b) plot  $n_e$  in the  $x - y$  and  $x - z$  planes. (c) is a plot of  $E_z$  in the  $x - y$  plane. (d) is the  $x - p_x$  phase space, looking only at electrons with  $p_x > 1.5 \text{ MeV}$ . In (e), (d) has been integrated along its spatial dimension to produce an electron spectrum.

soliton structures can be formed in the ‘high density’ LWFA’s necessitated by low energy drive pulses. At the time of their creation a large charge of few MeV electrons is accelerated 2D simulations also strongly suggest that postsoliton formation can result in the injection and acceleration of a few MeV electron beam.

## 5 Conclusion

We presented a review of LWFA scaling laws and determined that while long wavelength drive pulses must be more energetic for the same level of electron acceleration, this can be compensated by a higher injected charge. Additional advantages include a larger wakefield, which would be beneficial for diagnostics, and removing the re-

quirement for very small targets, which are more difficult to produce.

Results of 2D PIC simulations of LWFA’s driven by a 25 mJ, 30 fs, 4  $\mu\text{m}$  laser pulse were shown. These are the proposed operating parameters of the 10 Hz mid-infrared Chimera laser system currently under construction at Imperial College London. The optimal plasma parameters were found for self-injecting LWFA’s, suggesting that Chimera could drive a tabletop source of 20-40 MeV electron beams, accelerated in millimetre-scale targets. We also found that for comparatively high  $n_e/n_c$  there is a large red shift of the laser pulse, and that the long wavelength light can have a slightly sub-TV electric field. This light continues to drive a cavitated wakefield bubble after the depletion of the initial drive pulse. Some of the light becomes so redshifted that the plasma is opaque to it and it becomes trapped, resembling the formation of postsolitons. A large population of electrons is injected into the approximately stationary postsoliton bubble and is accelerated up to 5 MeV. This effect was confirmed in 3D simulations. This has potential to be a bright source of few MeV electrons.

## Acknowledgements

The authors acknowledge support from AFOSR (FY15 MURI Topic 13), and was also supported by STFC grant numbers ST/J002062/1, ST/P000835/1 and ST/P002021/1. We acknowledge the use of the computational resources of the Imperial College Research Computing Service, DOI: 10.14469/hpc/2232.

## References

- [1] T. Tajima and J. M. Dawson. “Laser Electron Accelerator”. In: *Phys. Rev. Lett.* 43.4 (1979), pp. 267–270.
- [2] E. Esarey, C. Schroeder, and W. P. Leemans. “Physics of laser-driven plasma-based electron accelerators”. In: *Rev. Mod. Phys.* 81.3 (2009), pp. 1229–1285.
- [3] A. Pukhov and J. Meyer-ter Vehn. “Laser wake field acceleration: the highly non-linear broken-wave regime”. In: *Appl. Phys. B Lasers Opt.* 74.4–5 (2002), pp. 355–361.
- [4] W. Lu et al. “Nonlinear Theory for Relativistic Plasma Wakefields in the Blowout Regime”. In: *Phys. Rev. Lett.* 96 (2006), p. 165002.
- [5] S. Kneip et al. “Near-GeV Acceleration of Electrons by a Nonlinear Plasma Wave Driven by a Self-Guided Laser Pulse”. In: *Phys. Rev. Lett.* 103 (2009), p. 035002.

- [6] H. T. Kim et al. “Enhancement of Electron Energy to the Multi-GeV Regime by a Dual-Stage Laser-Wakefield Accelerator Pumped by Petawatt Laser Pulses”. In: *Phys. Rev. Lett.* 111.16 (2013), p. 165002.
- [7] X. Wang et al. “Quasi monoenergetic laser plasma acceleration of electrons to 2 GeV”. In: *Nat. Commun.* 4.1988 (2013).
- [8] W. P. Leemans et al. “Multi-GeV Electron Beams from Capillary-Discharge-Guided Sub-petawatt Laser Pulses in the Self-Trapping Regime”. In: *Phys. Rev. Lett.* 113 (2014), p. 245002.
- [9] Z. H. He et al. “High repetition-rate wakefield electron source generated by few-millijoule, 30 fs laser pulses on a density downramp”. In: *New J. Phys.* 15 (2013).
- [10] B. Beaurepaire et al. “Effect of the laser wave front in a laser-plasma accelerator”. In: *Phys. Rev. X* 5.3 (2015), pp. 1–7.
- [11] D. Guénöt et al. “Relativistic electron beams driven by kHz single-cycle light pulses”. In: *Nat. Photonics* 11.5 (2016), pp. 293–296.
- [12] D Gustas et al. “High-charge relativistic electron bunches from a kHz laser-plasma accelerator”. In: 013401 (2017), pp. 1–7.
- [13] W. Lu et al. “Generating multi-GeV electron bunches using single stage laser wakefield acceleration in a 3D nonlinear regime”. In: *Phys. Rev. Spec. Top. - Accel. Beams* 10.6 (2007), p. 061301.
- [14] A. Buck et al. “Real-time observation of laser-driven electron acceleration”. In: *Nat. Phys.* 7.7 (2011), pp. 543–548.
- [15] A Sävert et al. “Direct Observation of the Injection Dynamics of a Laser Wakefield Accelerator Using Few-Femtosecond Shadowgraphy”. In: *Phys. Rev. Lett.* 055002.July (2015), pp. 1–5.
- [16] C. J. Zhang et al. “Femtosecond Probing of Plasma Wakefields and Observation of the Plasma Wake Reversal Using a Relativistic Electron Bunch”. In: 064801.August (2017), pp. 1–6.
- [17] D. Papp et al. “Laser wakefield acceleration with high-power, few-cycle mid-IR lasers”. In: *Nucl. Instruments Methods Phys. Res. Sect. A Accel. Spectrometers, Detect. Assoc. Equip.* January (2018), pp. 1–4.
- [18] P. Sprangle, C. M. Tang, and E. Esarey. “Relativistic self-focusing of short-pulse radiation beams in plasmas”. In: *IEEE Trans. Plasma Sci.* 15.2 (1987), pp. 145–153.
- [19] T. D. Arber et al. “Contemporary particle-in-cell approach to laser-plasma modelling”. In: *Plasma Phys. Control. Fusion* 57 (2015), p. 113001.
- [20] J. T. Mendonça and L. Oliveira E Silva. “Regular and stochastic acceleration of photons”. In: *Phys. Rev. E* 49.4 (1994), pp. 3520–3523.
- [21] W. B. Mori. “The physics of the nonlinear optics of plasmas at relativistic intensities for short-pulse lasers”. In: *IEEE J. Quantum Electron.* 33.11 (1997), pp. 1942–1953.
- [22] I. Kostyukov, A. Pukhov, and S. Kiselev. “Phenomenological theory of laser-plasma interaction in bubble regime”. In: *Phys. Plasmas* 11.11 (2004), p. 5256.
- [23] N. M. Naumova et al. “Formation of electromagnetic postsolitons in plasmas”. In: *Phys. Rev. Lett.* 87.18 (2001), pp. 185004–1–185004–4.
- [24] G. Sarri et al. “Observation of Postsoliton Expansion Following Laser Propagation through an Underdense Plasma”. In: *Phys. Rev. Lett.* 105.17 (2010), p. 175007.